Macromolecules

Article

pubs.acs.org/Macromolecules

Structural Studies of Polyaramid Fibers: Solid-State NMR and First-Principles Modeling

J. Ole Brauckmann,[†,‡,⊥] Pegah Zolfaghari,[‡,⊥] René Verhoef,[§] Enno A. Klop,[§] Gilles A. de Wijs,[‡] and Arno P. M. Kentgens*[,‡]

[†]TI-COAST, Science Park 904, 1098 XH Amsterdam, The Netherlands

[‡]Institute for Molecules and Materials, Radboud University, 6500 GL Nijmegen, The Netherlands

[§]Teijin Aramid Research Institute, P.O. Box 5153, Arnhem, The Netherlands

Supporting Information

ABSTRACT: Aramid fibers are of practical interest due to their high tensile strength, high elastic modulus, low elongation at breakage, and thermomechanical stability. Here we combine high-resolution solid-state NMR and density functional theory (DFT) calculations to gain insight into the details of the molecular packing of *p*-phenylene terephthalamides (PPTA). On the basis of the four models discussed thus far in the literature, we create a family of 16 possible structures. Calculations relate ^{1}H and ^{13}C chemical shifts obtained from experiments to structural aspects. Nucleus independent chemical shift (NICS) calculations show that ring currents and $\sigma-\pi$ interactions as well as hydrogen bonding influence the chemical shifts on the rings. We obtain an unambiguous assignment, which differs from the literature data for carbon, for all resonances relating to the repeating unit of PPTA and obtain new insights into the possible packings of the PPTA units within the unit cell.

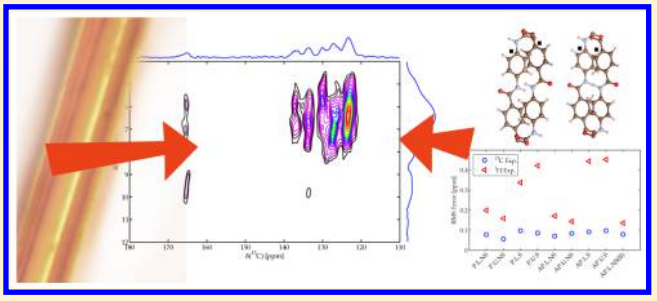

INTRODUCTION

Poly(*p*-phenylene terephthalamide) (PPTA) fibers are known for their exceptional mechanical and heat-resistant properties. They are sold under the commercial names of "Twaron" and "Kevlar". The packing of the fibers into a solid state crystal is thought to significantly impact the thermo-elastic properties of the fibers. Hence a complete understanding of the packing, in all its intricate details, is valuable. Many structural studies have been carried out (see below), mostly using X-ray diffraction (XRD).[1−6] Here we complement these and other studies with in-depth solid-state NMR characterization and computational modeling based on density functional theory (DFT).

The repeating unit of PPTA is shown in Figure 1. It consists of a terephthaloyl ring (t-ring, left) and a phenylene-diamine ring (p-ring, right). The unit cell comprises two chains. The cell parameters are well-known but the orientation of the two chains with respect to each other in the unit cell is under debate for a long time. Since the t- and the p-rings have very similar scattering amplitudes, X-ray diffraction (XRD) studies have difficulties to discriminate between different packings within the unit cell.

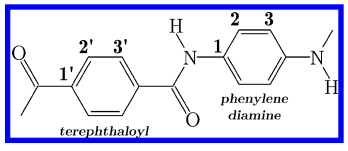

Figure 1. Repeating unit of poly(*p*-paraphenylene terephtalamide). The left ring is referred to as the terephthaloyl ring (t-ring), the right one as the phenylenediamine (p-ring). Atoms in the t-ring are numbered with a prime notation, while the atoms in the p-ring are not. Protons are numbered according to the labeling of the carbon they are attached to.

Aramid fibers are spun from lyotropic (liquid-crystalline) solutions of the polymer in sulfuric acid. Depending on the concentration of the solution two crystal modifications are observed.[5] When spun from low concentration a different molecular chain packing is seen, often referred to as the Haraguchi form or form II.[4,5] This form, however, cannot be obtained in a pure form. The prevalent form in high-modulus fibers is reported to have a pseudo orthorhombic unit cell. Most studies on the packing of the molecular chains are based on fiber XRD, whereas single-crystal electron diffraction and more recently fiber neutron diffraction have been used as well.[1,3−8]

The XRD studies were used to establish the packing of the chains relative to each other. Northolt and Tadokoro independently proposed two very similar structures based on fiber XRD.[1,3] In both studies, the chains within the unit cell are shifted about 0.5*c* with respect to each other. In the Northolt structure the shift is not exactly 0.5*c*, but one of the chains is slightly displaced (0.32 Å) lowering the symmetry compared to the Tadokoro structure. Subsequently Liu et al.[6] carried out single-crystal electron diffraction measurements. From these

Received: May 18, 2016
Revised: July 12, 2016
Published: July 27, 2016

DOI: 10.1021/acs.macromol.6b01051
Macromolecules 2016, 49, 5548−5560

measurements cell parameters similar to those of the earlier studies were derived, but the observed reflections agreed better with a structure with adjacent chains at the same height (alike rings next to each other). Later Plazanet et al.[8] studied PPTA using neutron vibration spectroscopy and DFT calculations. In the calculations another model, the Pb model, related to the Liu model, was introduced. Here adjacent chains in neighboring sheets are also at the same height, but the amide linkages have parallel configuration whereas the amide linkages in the Liu model are antiparallel.

Because polyaramid fibers do not dissolve in common organic solvents, the NMR studies in literature are either of PPTA in sulfuric acid (lyotropic solutions[9]) or solid-state NMR spectra. English et al. were the first to report a solid-state NMR ^{13}C chemical shift assignment for the six resonances observed for PPTA.[10] Furthermore, static variable temperature (VT) NMR measurements indicate that no high frequency ring flipping takes place over the temperature range from −170 to 200 °C. In hydrated samples of Kevlar-49, the splitting on the t-ring remains, indicating that also upon hydration at elevated temperatures of 80 °C, no fast flipping of the rings takes place and thus hydration does not affect the bulk structure of PPTA.[11] However, a fraction of carbons with shorter T_1 was noticed, suggesting the presence of an amorphous phase in Kevlar-49.

Besides structural studies, the dynamics[12−18] and molecular alignment[17,19,20] of the chains in PPTA fibers have been intensely studied. The orientational distribution of the chains was found to be of the order of 10°, with the actual value changing somewhat for different grades of PPTA.[17,19,20] For the amide, t-ring, and p-ring segments heterogeneous and slightly different dynamics are observed. For all the segments, these dynamics take place at the surface of the crystallites only, with the core being rigid on the NMR time scale. The studies described above convincingly show that NMR can be used to investigate the morphology and dynamics of PPTA at various temperatures. All studies confirm the high crystallinity of this polymer as suggested by XRD studies. Very recently Deshmukh et al. studied a family of mixed aromatic-aliphatic polyamids by XRD, solid-state NMR and DFT calculations.[21] The solid-state ^{13}C spectra of these samples clearly indicate the presence of an amorphous fraction. VT cross-polarization experiments show that the p-ring moves on the kHz scale, as motions interfere with polarization transfer. This is not observed in PPTA. This work presents the first DFT chemical shift calculations for PPTA for assignment purposes, however this study is limited to carbon chemical shifts of an isolated PPTA-fragment in the gas-phase. Therefore, no information about molecular packing can be obtained from these calculations.

In summary, the structure of PPTA is well-known with respect to cell parameters and chain conformation.[1,8,22] However, the relative displacement of the chains and the orientation of hydrogen bonds between amide linkages are not exactly known. Because of the presence of several aromatic units, having strong ring-current effects, the solid-state NMR chemical shifts in PPTA are expected to be very sensitive to packing effects. Hence different packings of the two chains in the unit cell should translate into substantial chemical shift differences. Therefore, NMR shifts will be sensitive to the structural variations of the different models discussed in the XRD studies described above which we explore in the present study. We anticipate that these structural variations will also be reflected in heteronuclear correlation experiments (HetCor). Shorter nuclear distances correspond to a stronger dipolar interactions and thus more intense peaks in a HetCor spectrum. In HetCor experiments mostly intramolecular correlations are visible, since intermolecular distances are often larger and therefore invisible due to dipolar truncation. From the experiments alone, no information on the packing can be deduced and therefore calculations of structural models are needed to relate chemical shifts obtained from intramolecular correlations to different packings of the molecules or structural models. In this study we establish an assignment of the proton and carbon resonances, with the help of high-resolution solid-state NMR experiments at high field (20 T), using HetCor experiments. We relate the resonance assignments to structural models via their chemical shifts obtained by DFT calculations. We consider a comprehensive family of structures derived from the models discussed thus far in literature and study their energetics using DFT calculations. In the following we discuss the rationale in formulating the various structural models considered, before evaluating the results obtained by solid-state NMR. By comparing experimental results with the calculations, we get new insight into the possible allomorphs of PPTA.

MATERIALS AND METHODS

Computational Methods. We performed density functional theory (DFT) calculations[23,24] using the PBE generalized gradient approximation (GGA)[25] and the projector augmented wave method (PAW)[26,27] as implemented in the Vienna *ab initio* Simulation Package (VASP).[28,29] A Γ-centered 4 × 5 × 3 Monkhorst−Pack grid of *k*-points for sampling the Brillouin zone was used.[30] The experimental lattice constants and atomic position were used as a starting point for structural relaxation. The lattice parameters and atomic positions were relaxed until the total energy changed by less than 10^{-6} eV and residual force was less than F_{max} = 0.01 eV/Å. An energy cutoff of 600 eV has been used for full relaxation and self-consistent electronic calculations. For hydrogen atoms an all-electron PAW data set was used whereas for C, O and N the 1s core states were kept frozen.

In order to include van der Waals (vdW) interactions we use the nonlocal vdW-DF[31−33] correlation functional as implemented in VASP[34,35] using the algorithm of Román-Pérez and Soler.[36] In the following we briefly summarize the functionality of vdW-DF. In vdW-DF the exchange-correlation energy is partitioned as

$$E_{xc} = E_x + E_c^{vdW} + E_c^{loc} \quad (1)$$

In the original vdW-DF method,[31] E_x is the revPBE exchange functional.[37] The second term, E_c^{vdW}, accounts approximately for nonlocal electron correlation effects (i.e., dispersion). The final term, E_c^{loc}, is the local correlation energy for which the local density approximation (LDA) was used. A large number of other options for the exchange part E_x of the functional have been proposed, including the optPBE-vdW, optB88-vdW, and optB86b-vdW functionals, in which the exchange functionals were optimized for the correlation part[34] and the vdW-DF2 of Langreth and et al.[38]

We tested the vdW-DF[31−33] for benzene with the optB88-vdW and optB86b-vdW functionals and also with the vdW-DF2 method[38] in which a modified vdW kernel along with the PW86 exchange functional[39] was used. We found the results of the calculation for vdW-DF2 functional for benzene in good agreement with the experiments,[40] both for the cohesive energy and lattice parameters (Table S1). Therefore, for the structural optimization of the PPTA models, we used rPW86 exchange functional.

Chemical Shielding Parameters. The NMR chemical shielding parameters were calculated with the Gauge-including PAW (GIPAW) linear response[41,42] method using pure PBE[25] and the standard PAW data sets for VASP.5.2.[43] A kinetic energy cutoff of 600 eV on the plane wave basis set was applied and a Γ-centered 4 × 5 × 3 *k*-point mesh was used. For one of our models we checked the effect of using hard PAW data sets. There was no significant effect on the shielding.

Nucleus Independent Chemical Shift (NICS) and Chemical Interactions Between the Molecules. We used the Nucleus Independent Chemical Shift (NICS) approach to understand crystal

DOI: 10.1021/acs.macromol.6b01051
Macromolecules 2016, 49, 5548−5560

packing effects and chemical interactions occurring in the crystal. Here we remove a molecule (in fact, a polymer chain) from an appropriate super cell and calculate the chemical shifts δ_{NICS} at the nuclear sites of the removed molecule as well as the chemical shifts $\delta_{molecule}$ of the isolated molecule only. In case there would be no chemical interaction between the molecule and its surroundings the shift of the crystal $\delta_{crystal}$ would just be a simple sum:

$$\delta_{crystal} = \delta_{molecule} + \delta_{NICS}$$

However, in case of intermolecular interactions between the molecule and its surroundings there is an additional contribution $\delta_{interacting}$

$$\delta_{crystal} = \delta_{interacting} + \delta_{molecule} + \delta_{NICS}$$

We obtain the intermolecular interaction $\delta_{interacting}$ as the difference between the calculated $\delta_{crystal}$ and calculated $\delta_{molecule} + \delta_{NICS}$:

$$\delta_{interacting} = \delta_{crystal} - (\delta_{molecule} + \delta_{NICS}) \quad (2)$$

We apply this approach to analyze the ^{1}H chemical shifts of our models. To prevent interactions between the cavity created by the removed molecule and its images that arise from the periodic boundary conditions (PBC) in our calculations, a $2 \times 2 \times 1$ supercell is employed. The same size supercell was used for the shift calculations of the crystal and the molecule, in order to remove any remaining small effect of the PBC. An energy cutoff of 600 eV and only the Γ-points were used for crystal, crystal with cavity and molecule.

Experimental Section. The sample studied here is Twaron 1010 supplied by Teijin Aramid. The fibers were thoroughly dried in an oven at 130 °C for at least 24 h and cut in small pieces for NMR measurements. All spectra were recorded on a Varian VNMRS 20 T (850 MHz) solid-state NMR spectrometer using a Varian 1.6 mm HXY fast MAS probe. For CP the ^{13}C B_1 field was calibrated to 50 kHz. The ^{1}H field was matched at the +1 Hartmann−Hahn condition (~85 kHz). For the CP spectra the contact times are indicated in the figures. For the heteronuclear correlation (HetCor) spectra a contact time of 500 μs was used. The relaxation delay was set to 10 s. During acquisition SPINAL64[44] decoupling at 128 kHz was used. The spectral width in the indirect dimension was fixed to half the spinning frequency (ν_r= 35.04 kHz) and 48 t_1-increments with 64 averages and states phase encoding were recorded. Carbon chemical shifts are reported relative to TMS, using the methylene resonance of solid adamantane (38.48 ppm)[45] as external chemical shift reference. For protons, the resonance of adamantane (1.74 ppm)[46] was used as external reference.

STRUCTURAL MODELS

Structural Models From Literature. Two forms of crystal packings have been proposed for PPTA referred to as form I and form II.[1,4,6,22,47,48] The formation of the different forms (I vs II) depends on the processing details.[1,4,22,48] The chains in form I and form II are aligned approximately along the fiber axis, *z*. In the *x,y* plane, they are located at 0,0 and $\frac{1}{2}$, $\frac{1}{2}$ for form I and at 0,0 and $\frac{1}{2}$, 0 for form II.[1,4,6,22,47,48] Since the diffraction data in the literature are focused on form I and form II cannot be obtained in a pure and stable form, we have focused our attention to form I models of the fiber.[1,6,10] For form I, different structures with very similar cell parameters have been reported. The first structure for PPTA was proposed in 1973 independently by Northolt and Tashiro et al. based on X-ray fiber diffraction experiments.[1−3] It is known as the Northolt model. The Northolt structure has a monoclinic (pseudo-orthorhombic) unit cell that possesses *Pn* or $P2_1/n$ space group symmetry. Later, in 1996, Liu et al. reported a structure obtained from electron single-crystal diffraction measurements.[6] It is known as the Liu model. From the measurements, similar cell parameters as for the Northolt model were derived, but the observation of relatively strong 210 reflections as well as 120, 320, and 410 reflections agrees better with a structure where adjacent chains are at the same height (alike aromatic rings next to each other). In a more recent study by Gardner et al.,[7] using neutron fiber diffraction of a selectively deuterated sample, the Liu model was confirmed. Plazanet et al. studied PPTA by neutron vibration spectroscopy and compared the results to structural models of PPTA and theoretical neutron vibration spectra by density functional theory (DFT).[8] In the calculations a symmetry related version of the Liu model, the so-called Pb model, was included. In this model, the amide linkages of the neighboring chains are in a parallel configuration, whereas the Liu model has an antiparallel configuration.

Family of Possible Structures. The four structural models discussed above have a very similar unit cell, the aromatic rings in adjacent sheets are in a herringbone packing and the chains are related by only one (pseudo) glide symmetry operation that transfers one chain in the unit cell into the other. They differ in three structural aspects within the unit cell: the orientation of the amide linkage, whether like or unlike aromatic rings are next to each other (translation of 0.5*c* of one of the chains) and the presence or absence of a slight shift of a fraction of an Ångstroms of one of the chains along *c*. A schematic view of these modifications is shown in Figure 2.

The four models discussed this far are not the only conceivable structures for PPTA form I. In principle, we can construct a family of 16 structures within the unit cell by systematically combining the four pairs of structural motifs described above: First, herringbone packing (**HP**) or similar packing of the phenyl rings between sheets (**SP**), second, parallel (**P**) or antiparallel (**AP**) alignment of amide linkages, third, like (**L**) or unlike (**U**) neighboring aromatic rings in adjacent chains, and finally, a small shifting (**S**) or no-shift (**NS**) of adjacent chains. Using this

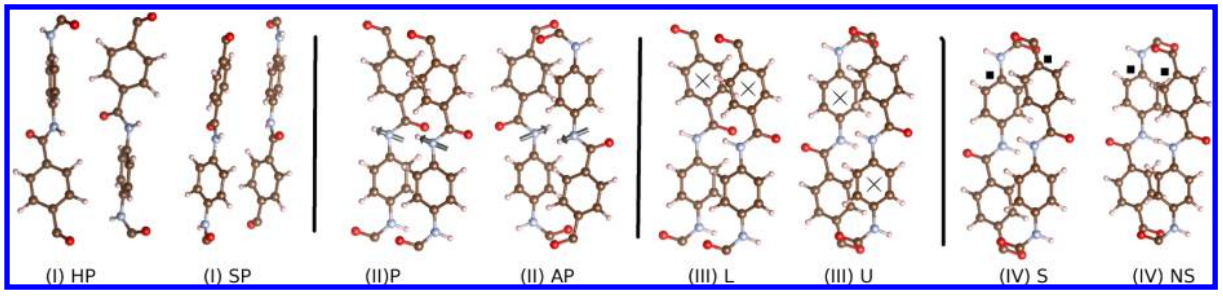

Figure 2. Schematic labeling of PPTA structures used in this work is depicted above. (I) **HP** and **SP** stand for herringbone and similar packing of the aromatic rings in adjacent chains. (II) **P** and **AP** stand for parallel or antiparallel orientation of amide linkage, respectively. (III) **L** and **U** indicate whether like or unlike aromatic rings are next to each other in adjacent layers. (IV) **S** and **NS** stand for a small shift from exactly 0.5*c* displacement or no-shift of neighboring chains.

DOI: 10.1021/acs.macromol.6b01051
Macromolecules 2016, 49, 5548−5560

nomenclature the "Northolt"-model with *Pn* space group has herringbone packing (**HP**), parallel alignment of the amide linkages (**P**), unlike neighboring aromatic rings in adjacent chains (**U**) and finally, a small shift of the adjacent chains (**S**) is therefore referred to as HP.P.U.S. Similarly the Northolt model with $P2_1/n$ space group can be referred to as HP.AP.U.S, the Liu model as HP.AP.L.NS, and the Pb model as HP.P.L.NS. In all 16 models, there is still one symmetry operation relating the two chains in the unit cell. For the **S**-models, however, the inversion centers on the aromatic rings are lost.

We fully relaxed the 16 potential structures obtained by systematic combinations of the structural modifications proposed for PPTA. After relaxation only eight different models are energetically viable. Deviation from the herringbone packing resulting in a similar packing (**SP**) of the aromatic rings is energetically unfavorable. In fact for all the **SP**-models the total energy is ∼13 meV/atom higher compared to the herringbone variants. Since all eight remaining structures keep the herringbone packing (**HP**), we remove this tag and keep the combination of three structural aspects. The energy of these eight structures is reported in Table 1. In terms of total energy, the remaining structures are very similar and therefore all viable candidates for the structure of PPTA.

Table 1. Total Energy per Atom of the Eight Optimized Structures of PPTA

structures		energy (eV/atom)
AP.U.S		−5.9365
AP.U.NS		−5.9362
AP.L.S		−5.9350
AP.L.NS		−5.9360
P.U.S	≅Northolt	−5.9348
P.U.NS		−5.9340
P.L.S		−5.9357
P.L.NS	≅Pb	−5.9352

It is worth mentioning that the AP.L.NS structure can have two different forms: The main variant AP.L.NS has a β-angle of approximately 104°. This is the one we obtain after structural relaxation and its energy is listed in Table 1. It is the only of the eight structures that has a β-angle substantially different from 90°. The other, AP.L.NS(II), has $\beta = 90°$. Although AP.L.NS(II) is unstable, as it relaxes to AP.L.NS, when using a (too) low cutoff of 400 eV, its β-angle does not relax. So we keep AP.L.NS(II) using a structure optimized at 400 eV, since it is the structure that strongly resembles the Liu model that is widely discussed in the literature.[3,6,8] Therefore, after relaxation, the total number of considered structures is 17. Out of them, nine structures are viable candidates, which are taken into account in the remainder of this study. Since these structures are very similar, we refer to them hereafter as allomorphs. Since all the structures are relaxed, all the allomorphs reported here are different from structures reported in literature. In the Supporting Information, we report for the nine most favorable allomorphs in terms of energy the lattice parameters and the coordinates of all the atoms in the unit cell.

RESULTS AND DISCUSSION

Solid-State NMR Experiments. The experimental chemical shift data were obtained for Twaron 1010 fibers, a PPTA yarn with intermediate modulus. We recorded ^{13}C CP spectra at different contact times to identify the quaternary carbons. In CP spectra, polarization is transferred through space through the heteronuclear dipolar interaction and therefore carbons close to protons are more pronounced at short contact times, compared to quaternary resonances. English et al. were the first to report a solid state ^{13}C chemical shift assignment of PPTA.[10] Six distinct resonances were observed and assigned by comparing them to spectra of dissolved PPTA and reference compounds. By dipolar dephasing the resonances around 166, 137.3, and 134.1 ppm were identified as quaternary carbons (carbons with no proton attached, carbonyl, 1 and 1′).[10] The resonance at 134.1 ppm was assigned to the t-ring and the resonance at 137.3 ppm to the p-ring. Then by intensity ratios, the resonances at 130.3 and 127.7 ppm were assigned to the ortho resonances on the t-ring (2′ and 3′). The remaining resonance at 123.8 ppm was assigned to the ortho resonances on the p-ring (2 and 3). The splitting of the resonances on the t-ring (2′ and 3′) was attributed to an approach of the amide proton to one of the carbons on the ring.

Since the 3D packing of the atoms is not reflected in the figure, we feel urged to explain that the position C2′ is defined as the carbon being closest to the oxygen of the carbonyl group. The C3′ on the other hand is much closer to the N−H proton. On the p-ring, the C2 position is the one closer to the NH proton and the remaining carbon is the C3 compare inset (Figure 3).

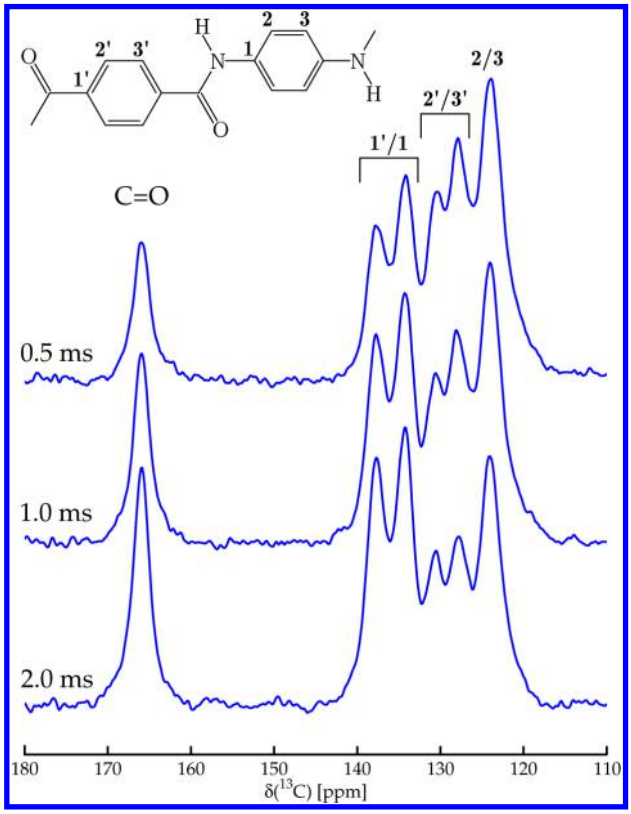

Figure 3. CP ^{13}C spectra of Twaron 1010 at 35 kHz MAS. At longer contact time the quaternary resonances are more pronounced (135−166 ppm). The spectra were recorded using 512 scans for each contact time with a recycle delay of 10 s.

This nomenclature is based on the labeling in the literature.[11] We note that depending on the 3D packing also all carbons can be inequivalent. Our experiments in Figure 3 confirm the assignment of English and Fukuda.[10,11] The resonances at 166, 137.6, and 134.2 ppm are clearly the quaternary resonances (carbonyl, 1′ and 1) since they increase in intensity at longer

DOI: 10.1021/acs.macromol.6b01051
Macromolecules 2016, 49, 5548−5560

polarization times. Then again by intensities, the remaining three resonances at 130.9, 127.9 are assigned to the aromatic carbons on the t-ring (2′ and 3′). The remaining resonance at 123.5 ppm is assigned to the ortho carbons on the p-ring (2 and 3). The higher intensity of this resonance is in agreement with the fact that the resonance belongs to four carbons in the structure, while the resonances at 130.9 and 127.9 ppm each represent two carbons.

Solely based on the chemical shifts we cannot assign the quaternary resonances 1 and 1′ to the different aromatic rings. Furthermore, we cannot assign the ortho-resonances on the t-ring to a position on the ring (2′ and 3′). The carbon resonances are relatively broad and thus we cannot conclude - solely based on the 1D carbon spectra, which allomorphs are present in the sample.

We expect that the proton chemical shifts will be more sensitive to the packing of the molecular chains in the unit cell since they extend from the aromatic rings and are more sensitive to changes in the structure, resulting for instance in altered ring currents effects of the neighboring chain. Therefore, we recorded a $^{1}H-^{13}C$ heteronuclear correlation spectrum (HetCor) with a short contact time of 500 μs to limit spin diffusion and thus only get correlations for the closest proton carbon distances. In Figure 4 the $^{1}H-^{13}C$ HetCor of Twaron fibers at 35.04 kHz

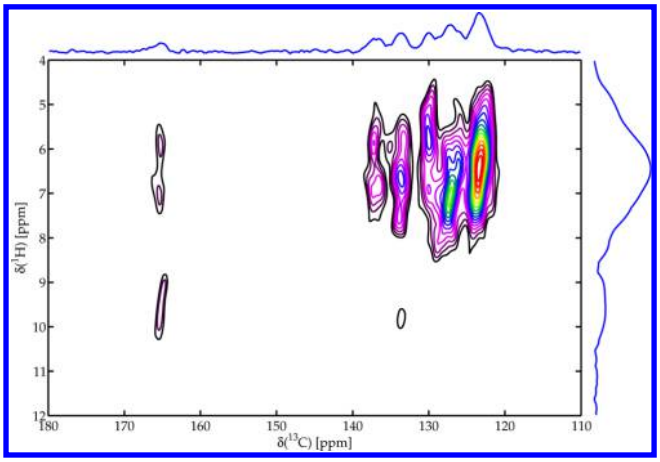

Figure 4. HetCor of Twaron 1010 recorded at 20 T using 35 kHz MAS. 48 t_1-increments were recorded in a spectral width of 17.5 kHz using 64 scans per increment and a recycle delay of 10 s. The projections are the skyline projections of the depicted region.

MAS at 20 T is shown. The traces displayed at the top and at the right are the skyline projections of the carbon and the proton dimension. The proton projection shows that even at 35 kHz MAS, the aromatic proton resonances still strongly overlap. In the individual carbon traces of the correlation spectrum clearly different proton chemical shifts become visible, showing that the aromatic protons have different chemical shifts that are not visible in single pulse excitation proton spectra. The more accurate ^{1}H chemical shifts available in the 2D experiment allow an assignment of most resonances. Starting in the carbon dimension from left to right, the carbonyl is relatively isolated and shows three proton contacts originating from the amide proton (9.6 ppm) and two resonances on the t-ring (5.7 and 7.2 ppm) corresponding to H2′ and H3′. The quaternary resonance at 137.6 ppm shows a similar pattern and is thus assigned to the quaternary resonance on the t-ring (C1′). The quaternary resonance at 134.2 ppm couples to overlapping aromatic proton resonances around 6.5 ppm and a weak contact to the amide proton, not visible for the resonance at 137.6 ppm, also in line with a larger $^{1}H-^{13}C$ distance for the C2′. This observation suggests that the assignment of the quaternary resonances C1 and C1′ reported by English and Fukuda in refs 10 and11 should be interchanged.

For the resonances at 130.9 and 127.9 ppm we observe a characteristic pattern: The resonance at 130.9 ppm shows a strong correlation to the proton resonating at 5.7 ppm and a weak one to the resonance at 7.2 ppm. For the carbons at 127.9 ppm, these intensities are reversed; a strong correlation to a proton at 7.2 ppm and a weak one to the protons 5.7 ppm arises. This pattern is characteristic for an aromatic ring with inequivalent proton and inequivalent carbon chemical shifts. Both proton traces show a strong and a weak interaction belonging to a close proton (the directly bound one) and a more distant proton (belonging to the neighboring carbon).

The proton trace at 123.5 ppm in Figure 4 shows no resolved individual resonances. The proton resonances are therefore tentatively assigned to 6.2 and 6.7 ppm for H2 and H3. This observation is supported by the observation of a strong correlation peak on the diagonal around 6.6 ppm in a ^{1}H single-quantum double-quantum (SQ-DQ) correlation experiment (Supporting Information).

The correlation allows the assessment of the proton chemical shifts of PPTA in the solid state. The proton chemical shifts on the t-ring differ more than on the p-ring (H2′/H3′ compared to H2/H3), as do the carbon chemical shifts (C2′/C3′ compared to C2/C3). The assignment from the experiment is summarized in Table 2.

These considerations do not yet allow a definitive assignment of the chemical shifts of the ortho carbons to a position on the t-ring, for which we resort to DFT calculations.

The splitting of the carbon resonances on the t-ring and the correlation pattern in the HetCor experiment are examples of the sensitivity of solid-state NMR to the local environments of the spins and thus to the packing of the molecular chains. In fact the splitting of the resonances on the t-ring is only observed in the solid state. When PPTA is dissolved in sulfuric acid, the splitting vanishes due to motional averaging.

Recent examples show that proton chemical shifts are more sensitive to structural changes and allow for better discrimination between structural models than do carbon chemical shifts.[49]

Table 2. Summary of the Chemical Shift Assignment Based on the Experiments of Twaron1010

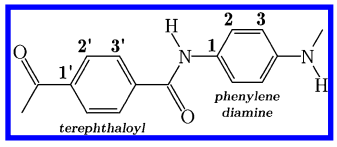

	1′	2′	3′	1	2	3	
^{13}C [ppm]	137.6	130.9	127.6	134.2	123.5	123.5	C═O: 166
^{1}H [ppm]	–	5.7	7.2	–	6.2/6.7	6.2/6.7	NH: 9.6

DOI: 10.1021/acs.macromol.6b01051
Macromolecules 2016, 49, 5548−5560

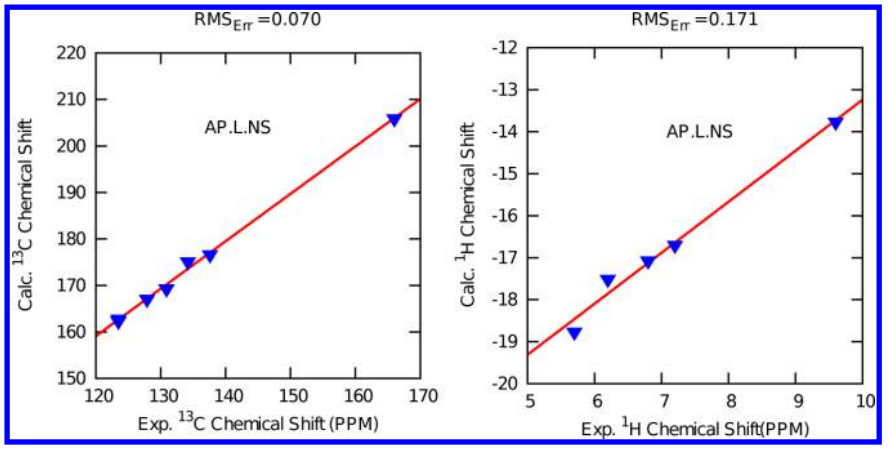

Figure 5. One-dimensional comparison of the experimental and calculated chemical shifts of the AP.L.NS allomorph.

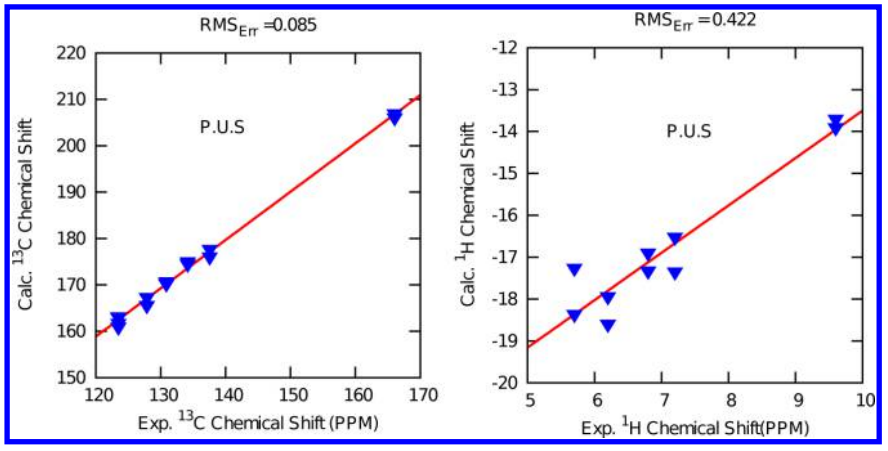

Figure 6. One-dimensional comparison of the experimental and calculated chemical shifts of the P.U.S allomorph.

Since the protons are on the outside of the aromatic rings in PPTA, we expect them to be very sensitive to packing effects in the solid state.

Chemical Shift Calculations. With the DFT calculations the chemical shifts can be related to different positions on the ring. This allows the identification of the C2′ carbon as the carbon on the t-ring being closest to the oxygen. It has the larger chemical shift (130.9 ppm, compared to 127.6 for the C3′).

We carried out chemical shift calculations for all 9 models described earlier. The calculations show variations of the chemical shift based on the different structural motifs:

- **P** vs **AP**
  Whether the amide bond is parallel or antiparallel has only a small effect on the chemical shifts of PPTA. The carbon chemical shifts hardly change, however the chemical shift difference of the protons on the t-ring (H2′ and H3′) increases for the antiparallel allomorphs. This is best seen in the 2D chemical shift comparison of the allomorphs with the HetCor experiment in Figure 10 and Figures S7−S15. Comparing the (P.*.*) and the (AP.*.*) allomorphs, the chemical shift difference of the H2′ and H3′ changes, indicated by the black arrows (Figure 10).
- **L** vs **U**
  The change of the aromatic ring in the adjacent chain (like or unlike) has a strong effect on the proton resonances of the p-ring. They resonate at higher ppm values for the unlike ring packing. This is also visible in the 2D comparison in Figure 10 and Figure 11, indicated by the blue arrows, and is visible in Figures S7−S15.
- **S** vs **NS**
  A shift of the chains relative to each other changes the symmetry of the resonances on the aromatic ring. Without shift of the neighboring chains, the carbons (and protons) on opposite sides of the same ring have the same chemical shift. A small shift of the chains causes large changes in the chemical shifts of the carbons and the protons. Especially the proton chemical shift varies strongly, regarding the smaller chemical shift range of protons. The carbons on the aromatic rings are not symmetry related anymore, and for all the carbons on the ring different resonances are seen. This can be clearly seen in the scatter from linearity for the (*.*.S) allomorphs, compared to the (*.*.NS) allomorphs (compare Figure 5 and Figure 6 and Figures S7−S15).

NICS Calculations and Intermolecular Interactions. In this section we aim to analyze to what extent the (calculated) chemical shifts and their differences among the structures are indicative of chemical interactions between the polymer chains. As an obvious first step, one can compare the isotropic chemical shift of a nucleus in the solid ($\delta_{crystal}$) with that of the same nucleus in an isolated molecule ($\delta_{molecule}$, keeping it in its crystal conformation), by calculating their difference $\delta_{stack} = \delta_{crystal} - \delta_{molecule}$. This approach has been successfully used, e.g., to investigate weak C−H···O bonding.[50] In PPTA this approach is not sufficient, because meaningful differences in chemical shift

DOI: 10.1021/acs.macromol.6b01051
Macromolecules 2016, 49, 5548−5560

are masked by ring-current effects. In order to remove these, we use δ_{NICS}. For example, instead of δ_{stack}, we use eq 2 and consider $\delta_{interacting} = \delta_{stack} - \delta_{NICS}$.[51]

If the electronic structure of the molecules is unaffected by the presence of their neighbors $\delta_{interacting}$ will be 0. So any deviation from 0 indicates an intermolecular chemical interaction (induction, hydrogen bond, etc.), albeit a weak interaction. The results for $\delta_{interacting}$ are compiled in Table 3.

Table 3. Calculated ^{1}H $\delta_{interacting}$ and the H to O Distance d_{OH} between Neighboring Molecules in the Hydrogen Bonded Sheets for the P.U.NS, AP.U.NS, AP.L.NS, and P.L.NS Models[a]

	H	$\delta_{interacting}$ (ppm)	d_{OH} (Å)
P.U.NS	2′	0.60	4.28
	3′	0.64	2.68
	2	1.17	2.83
	3	0.16	5.09
	N−H	1.67	2.07
AP.U.NS	2′	0.41	4.63
	3′	0.49	2.90
	2	0.96	2.58
	3	0.30	4.77
	N−H	1.48	2.12
AP.L.NS	2′	0.47	4.29
	3′	0.53	2.70
	2	0.81	2.88
	3	0.16	5.58
	N−H	1.59	2.08
P.L.NS	2′	0.45	4.46
	3′	0.57	2.77
	2	1.12	2.68
	3	0.21	4.91
	N−H	1.65	2.07

[a] $\delta_{molecule}$, δ_{NICS} and δ_{stack} are listed in the Supporting Information, Table S14.

Evidently there is little difference between the structures considered, all follow the same trend. There is no apparent correlation with d_{OH}, the intermolecular O···H distances in the hydrogen bonded sheets), except for the NH proton. For this proton $\delta_{interacting}$ is large (1.5−1.7 ppm), which is to be expected because of the N−H···O hydrogen bond network that makes up the molecular sheets. Interestingly, for H2 it is also substantial, i.e. of the order of 1 ppm. For each structure $\delta_{interacting}$(H2) is the largest of all the carbon attached protons. Evidently this points to a chemical interaction: It might relate to a $\sigma-\pi$ interaction or originate from an indirect effect of the NH···O hydrogen bond. From the geometrical point of view, the former is more likely: the aromatic units form a herringbone packing and the H2 proton is located closest to the centers of the neighboring aromatic rings. However, the same holds for H2′, for which $\delta_{interacting}$ is considerably smaller.

In order to get more insight in the nature of the intermolecular interactions, we did additional calculations of $\delta_{interacting}$ for two hypothetical systems based the P.U.NS structure. To switch off the effects of hydrogen bonding, we removed in model I all HN−CO groups from the molecules surrounding the molecule that we study. That single molecule is unaffected and frozen in its crystal conformation. Of the surrounding molecules only the C_6H_4 rings remained. We saturated the dangling bonds with hydrogens; i.e., we made an environment of benzene molecules, fixed at the positions of the PPTA rings. In this model system we have (to a good approximation) only the effect of $\sigma-\pi$ interactions, as all hydrogen bonds have been removed. Indeed, in Table 4 we see a substantial effect for both H2 and H2′ in

Table 4. $\delta_{interacting}$ (ppm) for PPTA in the P.U.NS Structure and for the Hypothetical Model I and Model II to Evaluate the Effects of Hydrogen Bonding (I) and $\sigma-\pi$ Interactions (II), Respectively (See Text)

	PPTA	model I	model II
2′	0.60	0.83	−0.10
3′	0.64	0.32	0.60
2	1.17	0.98	−0.18
3	0.16	0.32	0.35
N−H	1.67	0.00	1.71

model I. Moreover, we see no effect at all for the NH proton. Therefore, we conclude that the $\sigma-\pi$ interaction is a relevant contribution to the chemical shifts of PPTA. The $\sigma-\pi$ interactions might actually be the structure directing force behind the herringbone packing that is clearly favored in these systems.

Next, we considered the complementary model II, where we prevent the possibility of $\sigma-\pi$ interactions and focus only on the hydrogen bonding. Here we removed the C_4H_4 rings from the surroundings and saturated the remaining dangling bonds with hydrogens, yielding COH−NH−CH_3 molecules. We kept two atoms from the ring, so that N keeps the same nearest neighbors as in the crystal. Here we see a large $\delta_{interacting}$ for N (Table 4, model II), which is almost equal to that calculated for the crystal. However, we also observe effects on the ring, some even negative, indicating that the electronic structure of the ring system is affected by the NH···O hydrogen bonds. With these two models, we cannot completely assign the different effects leading to $\delta_{interacting}$ for the PPTA crystals. Evidently, our models are only complementary to some extent. However, these models clearly show, that both effects, intermolecular $\sigma-\pi$ bonding and NH···O hydrogen bond formation are present and compete to affect the electronic structure of the PPTA rings.

Comparison Experiment and Calculations. In DFT calculations the (absolute) chemical shielding at the nucleus is obtained, whereas in experiments the chemical shift relative to a reference compound is reported. So, the experimental and DFT chemical shifts should—in principle—only differ by a constant.

However, in the literature depending on the method used and the nucleus studied, a small deviation from a linear slope of unity is observed.[52−56] While in the earlier literature this issue was often discussed or both methods were considered, in more recent literature it is often dismissed and the chemical shifts are related by an enforced slope of unity.[57−59] It was also discussed to calculate, similar to an external reference in the solid-state NMR experiments, a reference compound to relate to.[60] However, since these compounds are often very mobile (TMS, adamantane), this is also prone to errors. Another approach is to calculate a library of known compounds and relate the slope obtained from a simultaneous fit to the compound of interest.[56]

To relate the calculated and the experimental chemical shifts, we chose here to directly compare the numbers by plotting the calculated (absolute) chemical shift of the allomorphs against the experimentally observed chemical shifts and determine for each allomorph the best fit of the form:

$$\delta_{calc} = m\delta_{exp} + b \quad (3)$$

Here m is the slope, with b the offset in units of ppm.

DOI: 10.1021/acs.macromol.6b01051
Macromolecules 2016, 49, 5548−5560

In Figure 5 this comparison is made for the proton and the carbon chemical shifts of the AP.L.NS allomorph. For protons and carbons of the AP.L.NS allomorph good linearity is obtained when compared to the chemical shifts of the experiment. For the P.U.S allomorph in Figure 6 good linearity for the carbons is obtained, however a doubling of the carbon resonances is seen in the calculations. For the protons this is even more pronounced. All the protons in the repeating unit show different chemical shifts. The ^{1}H resonances of this allomorph agree less well with the experimental data as the predicted scatter in proton shifts is not observed experimentally. For all the allomorphs, a linear agreement of the carbon isotropic chemical shifts can only be obtained, when the carbon assignment derived from the HetCor experiment is used (Table 2). The ^{1}H and ^{13}C chemical shift comparison of all the allomorphs is shown in Figures S2−S5. In general for the (**.*.S) allomorphs a doubling of the resonances is observed similar to the ones shown in Figure 6. We note that the assignment of English and Fukuda (C1 and C1′ interchanged[10,11]) gives a clear deviation from linearity, thus the calculations also suggest the reassignment indicated by the through-space contact for one of the quaternary carbons in the HetCor of PPTA.

For the identification of the best structural model the chemical shifts of all the nuclei should be compared. To be able to compare proton and carbon chemical shifts simultaneously despite their completely different chemical shift range and their different number in the unit cell, we chose to calculate for each model the root-mean-square error per atom and nucleus in a way that protons and carbons weigh approximately equal: We combined the ^{1}H and ^{13}C chemical shift data by scaling the ^{1}H and ^{13}C chemical shifts to an equal range and then calculating the root-mean-square error (RMS_{Err}) per atom in units of ppm using eq 4:

$$RMS_{Err}^{X} = \sqrt{\frac{1}{N_X s_X^2} \sum_{i=1}^{N_X} (\delta_{exp,i} - \delta_{lin,calc})^2} \quad (4)$$

Here X is either ^{1}H or ^{13}C, N_X is the number of atoms X in the unit cell, s_X is the scaling factor of 10 (200/20) for X = ^{13}C and one for X = ^{1}H, $\delta_{exp,i}$ is the chemical shift from experiments, and $\delta_{lin,calc}$ are the linear chemical shift predictions based on eq 3. They are obtained by filling in m and b from the fit, i.e., $\delta_{lin,calc} = m\delta_{exp} + b$.

The RMS_{Err} of the proton and the carbon chemical shifts of the different allomorphs are compared in Figure 7. The allomorphs without applied shift (**.*.NS) have a much lower RMS error for the protons. For the carbons there is very little variation in RMS error. Evidently, the proton chemical shifts are more sensitive to the structural variations in the unit cell. The other motif in the unit cell (**U** vs **L** and **P** vs **AP**) are not clearly reflected in the RMS_{Err}. Comprehensive details on the chemical shift comparison for all allomorphs can be found in the Supporting Information, Figures S2−S6 and Table S11. The calculated chemical shifts δ_{calc} of all the allomorphs are also given in the Supporting Information (Tables S2−S10).

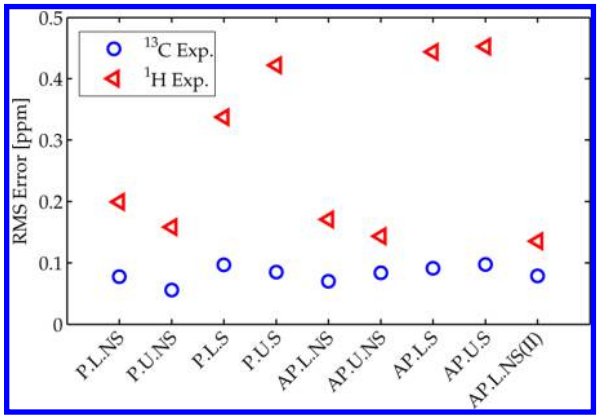

Figure 7. RMS error of the experimental proton and carbon chemical shift assignment in relation to all the models. Models which are not shifted show better agreement with the experimental assignment.

2D Comparison Experiment and Calculations. Above we compared the proton and carbon chemical shift data of different allomorphs separately. In principle the assignment is derived from a HetCor spectrum and therefore we aim to compare the chemical shifts of the allomorphs also in two dimensions. A full spin simulation of 56 atoms in a unit cell, with all the experimental parameters as the spinning speed, rf-fields, contact times etc. in it, is beyond the scope of this study. Therefore, we decided to compare only the chemical shift positions of the correlations we expect on the basis of the shortest distances and the number of atoms. In this way we ignore the intensity of the real spectrum but do not have to assume a line width for the allomorphs. Similar to the intensity the multiplicity of the atoms having similar chemical shifts weighs the comparison toward the more often occurring correlations.

With the assumption that only the through-bond ^{1}H,^{13}C contacts and the ^{1}H,^{13}C on the same ring (e.g., C2,H3, C1,H2/3) are visible in the HetCor, the 2D correlation of the experiment is well reproduced and consists of 30 peaks, many of them are overlapping. An example is shown for the AP.L.NS model in Figure 8 and compared to the assignment derived from the experiment.

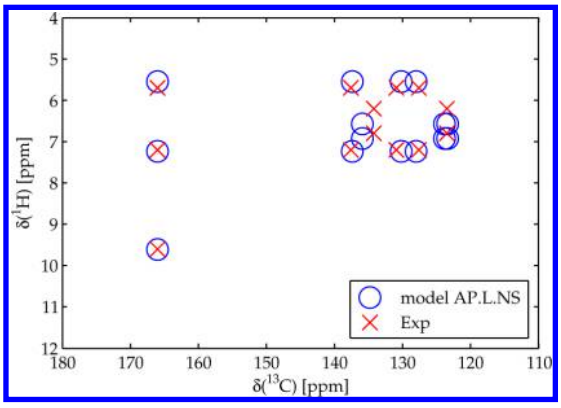

Figure 8. Comparison of the chemical shift assignment derived from the HetCor and the expected chemical shifts for the AP.L.NS model based on the shortest carbon−proton distances in the structure.

To quantify the agreement of the chemical shifts of an allomorph with the experimental assignment, we calculated all the possible distances between two pairs of correlations in the 2D spectrum. In this way we not only compare the distance of correlation peaks but also the relative distances between all the proton *and* the carbon resonances. Similar to the earlier discussion in 1D, we scale the carbon chemical shifts to an equal chemical shift range to prevent domination of the distance by their larger chemical shift range. The distances are calculated using eq 5

$$d_{ki} = \sqrt{\Delta\delta(^{13}C_s)_i + \Delta\delta(^{1}H)_i} \quad (5)$$

DOI: 10.1021/acs.macromol.6b01051
Macromolecules 2016, 49, 5548−5560

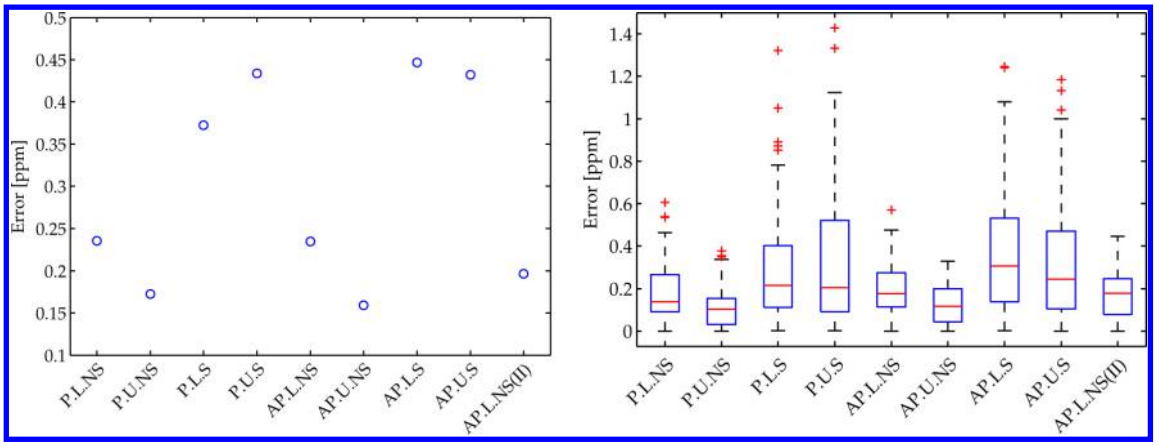

Figure 9. Left: 2D RMS Error of the experimental proton and carbon chemical shift assignment in relation to all the models. Models which are not shifted show better agreement with the experimental assignment. Right: boxplot of all the differences of distances (Δd_{ij}) between the experimental assignment and the allomorphs. A boxplot assumes a normal distribution of a variable. The red line indicates the median of the differences, the blue box indicates the range where 50% of the distribution is located (25th to 75th percentile), and the whiskers extend to $\pm 2.7\,\sigma$ (99.3%) of the distribution and outliers are indicated individually.

Here d_{ki} is a distance i between two correlation in spectrum k being either the experimental assignment or an allomorph. The subscript s indicates that the carbon chemical shifts are scaled (s equal to 10 as used previously). To obtain an RMS_{Error} the difference of the distances in an allomorph and the experiment is squared, summed, and normalized for the total number of distances considered:

$$\mathrm{RMS}_{Error,j} = \sum_{i=1}^{n} \sqrt{\frac{(d_{\mathrm{exp},i} - d_{ji})^2}{n}} \tag{6}$$

In eq 6, $RMS_{Error,j}$ is the RMS error of allomorph j calculated with n distances. The correlations of the carbonyl were neglected since these would give very large distances that could dominate the comparison. In total 24 of the 30 correlation peaks were considered, giving rise to 276 distances between them ($\binom{24}{2} = 276$). The 2D RMS error based on these distances per models is summarized on the left of Figure 9.

The trend of the error is very similar to the 1D RMS error, but it is based on the combined information on the proton and the carbon chemical shift. The fact that the trend in the 1D and 2D comparison is similar, indicates that the structural motifs are strongest reflected in the proton chemical shift. Also here the **.*.NS models have a lower RMS error. On first sight it looks as if the **U.NS** models have a lower RMS error and thus agree even better with the experiment (P.L.NS vs P.U.NS and AP.L.NS vs AP.U.NS). Since we have calculated 276 distances for all the models in this comparison, we can look in more detail at the deviations of the resonances of the allomorphs from the experiment. To see how strongly the **NS** and **S** models differ and whether the other structural motifs **AP** vs **P** and **L** vs **U** are reflected in the error, we look at the boxplot of the differences of the 276 distances ($\Delta d_{ij} = |d_{exp,i} - d_{ji}|$) (right of Figure 9).

The median of the differences shows a similar trend as the RMS error on the right, also here the **NS** models have a lower error. The much longer whiskers for the **.*.S models in the boxplots, show that these models agree much less than the **.*.NS models. Furthermore, the overlapping boxes of the **.U.NS vs **.L.NS allomorphs show that the differences are not significant.

Finally we compare the chemical shift positions and the intensities of all the allomorphs to the HetCor experiment (Figure 10 and Figure 11). For the intensities of the correlations we take the simple assumptions that indirect correlations have half the intensity of a direct correlation (e.g., a correlation of an aromatic carbon to the proton attached to the neighboring carbon C2/H3 vs C2/H2). Constituted HetCor spectra based on these assumptions and assuming line widths comparable to the experiment are shown in the Supporting Information and reproduce the 2D correlation from the experiment (Figures S7−S15). Here we neglect the line width and compare just the positions of the expected chemical shift correlations with the experiment. In total 30 correlations are considered. Overlapping correlations (shifts within 0.1 ppm) are summed and their total intensity is represented in the area of the dot.

For the five allomorphs having the **NS** motif, subtle differences are visible in the correlation patterns (Figure 10). The *.U.NS allomorphs (Figure 10, parts b and d), have the H2 and H3 correlations toward lower ppm values, whereas for the *.L.NS allomorphs they are at higher ppm (Figure 10 parts a and c). This is best seen when looking at the chemical shift difference of the protons on the t-ring and the p-ring indicated by the blue arrows in the figure. For the *.U.NS models, there is barely a difference, while for the *.L.NS models there is clear difference. We note for all the models that the H2/H3 resonance are similar in chemical shift, only the AP.L.NS(II) allomorph (Figure 10e) has a larger chemical shift difference (visible by the separated red dots in the trace at 123.5 ppm). The larger chemical shift difference agrees better with the broad proton trace observed in the experiment. For the **S** allomorphs shown in Figure 11 this is more subtle, since the proton and carbon resonances split, but still for the *.L.S allomorphs a larger chemical shift difference compared to the t-ring observed (Figure 11, parts a and b).

Comparing the **AP** and the **P** models, we note that the ^{1}H chemical shift for the H2′/H3′ decreases from about 1.5 ppm for the AP.*.NS to 1.1 ppm for the P.*.NS models. This change is indicated by the black arrows in the figure. The chemical shift difference of the P.*.NS models agrees better with the experiment as is best seen in the correlations of the carbonyl (166 ppm, Figure 10, parts c and d). Also the correlation pattern of the H2′/H3′ on the t-ring is reproduced by the **NS** allomorphs. All models show a strong-weak pattern for the trace of the

DOI: 10.1021/acs.macromol.6b01051
Macromolecules 2016, 49, 5548−5560

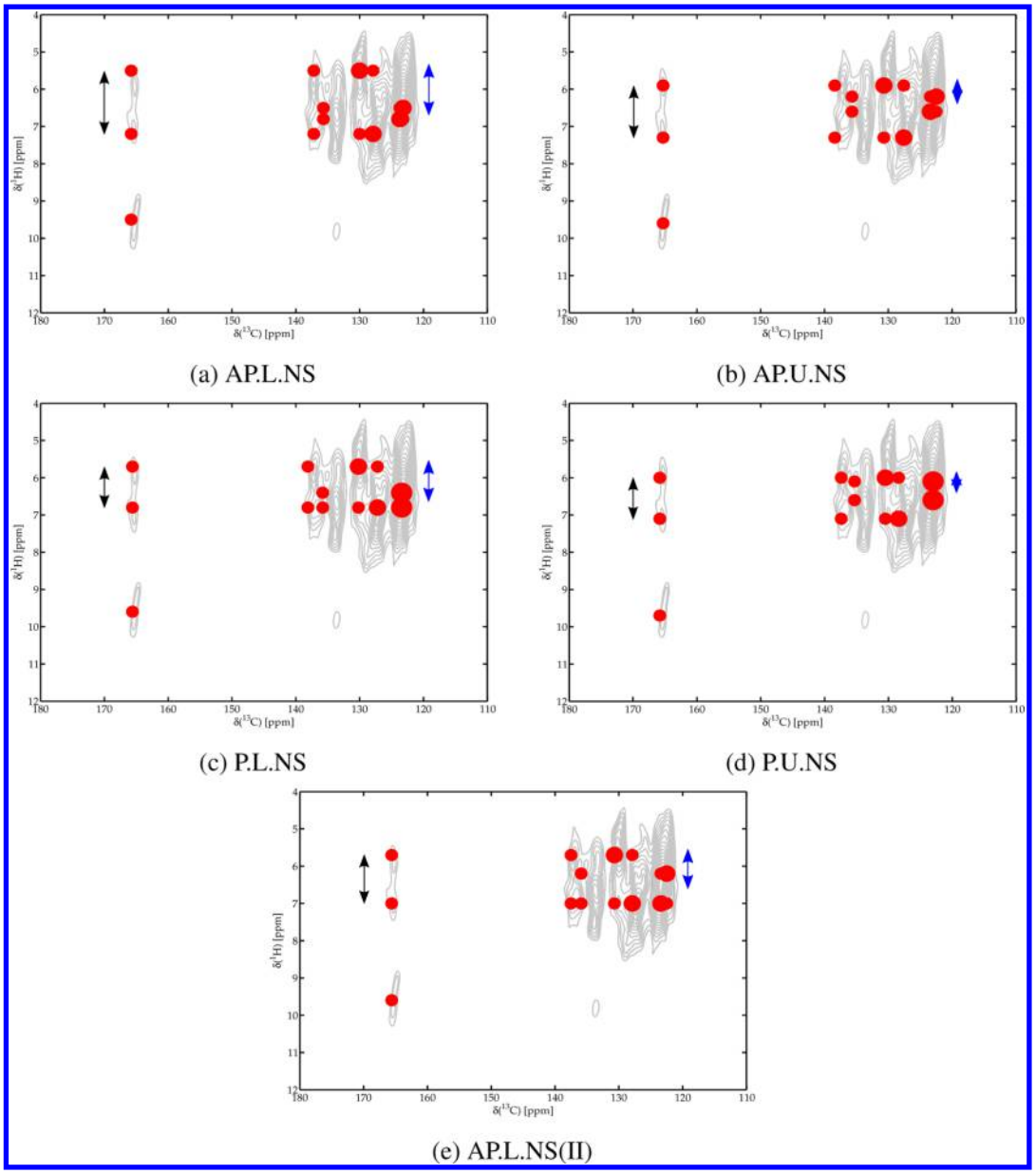

Figure 10. Comparison of the HetCor experiment (gray contours) with the correlations (red dots) for the **NS** allomorphs. Intensities are represented in the size of the dots and are based on the multiplicities and strength of correlations based on the shortest distances. Straight lines aid the comparison of peak positions in the **L** and **U** allomorphs. The black arrows indicate the chemical shift difference of the protons on the t-ring, and the blue arrows indicate the chemical shift difference between protons on the t-ring and the p-ring.

C2′/C3′ carbons (127−130 ppm). This pattern is not reproduced by the **S** allomorphs shown in Figure 11). The carbonyl correlations of the **S** models show less structure than the experiment and all carbon and proton resonances split, giving rise to different intensity distribution of the correlations. The H2′/H3′ correlations of the **NS** allomorphs are in line with the clear structure of three contacts observed in the carbonyl trace in the experiment.

Qualitatively the P.*.NS models agree best with the experiment, however these models also show clear differences to the experiment: the width of the proton correlation of the C2/C3 carbons is not matched in any of the **NS** allomorphs. The dots do not cover the contours of the experiment. Also the position of the C1 quaternary resonances does not agree with the position in the experiment. The rather broad H2/H3 correlations is not matched by a single **NS** allomorph. A broadening of the proton traces on the p-ring could also arise if two allomorphs of the group having *.L.NS and *.U.NS nomenclature are present. This would give rise to broadening of the proton trace of C2/C3 carbons, without much effect on the patterns of other correlations. The fact that there is no single model agreeing best is in line with the very similar total energy of the models and makes it probable that allomorphs coexist in the fibers. Hints for different structures simultaneously present in the fiber are not only the longstanding discussion in XRD literature,[1,3−6] but also the heterogeneous dynamics in PPTA observed by deuteron NMR.[12−17] These studies clearly reveal heterogeneous dynamics linked to a rigid/static fraction ascribed to the core and a dynamic fraction located at the surface of crystallites in PPTA. It was estimated that in as polymerized PPTA due to the small crystallite size the fraction at the surface is approximately 40%. Upon polymerization, the fraction decreases but a fraction remains

DOI: 10.1021/acs.macromol.6b01051
Macromolecules 2016, 49, 5548−5560

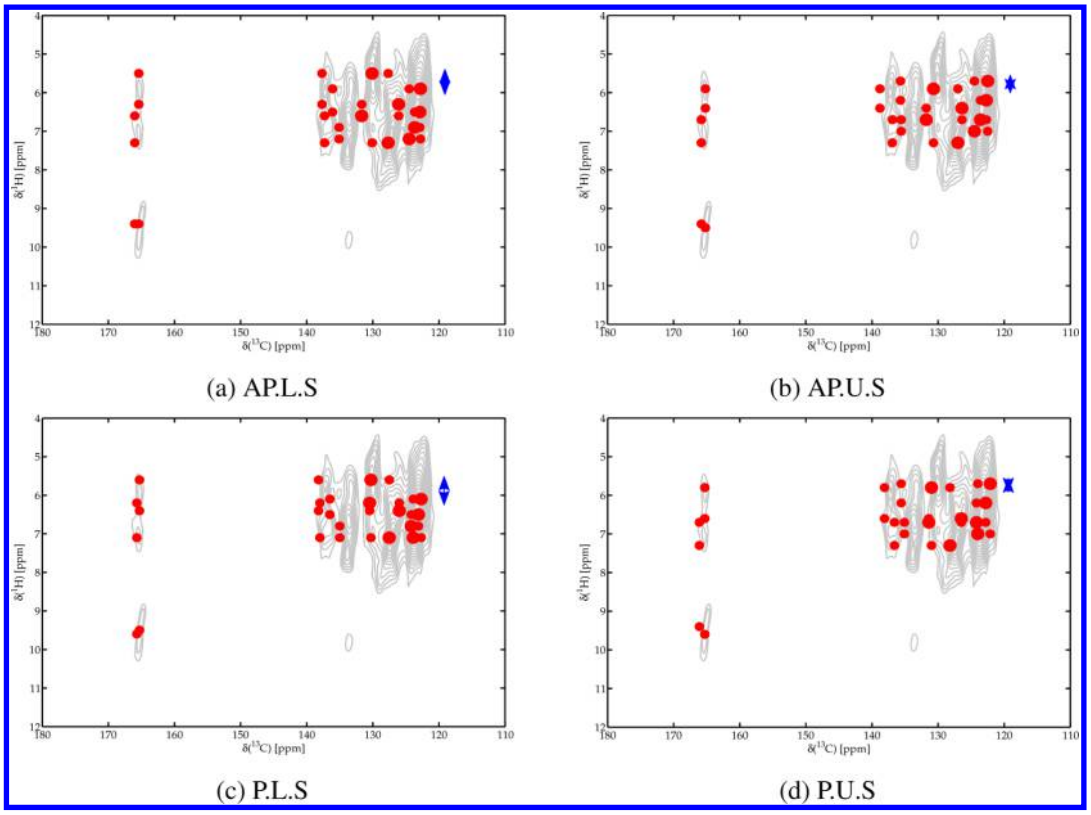

Figure 11. Comparison of the HetCor experiment (gray contours) with the correlations (red dots) for the **S** allomorphs. Intensities are represented in the size of the dots and are based on the multiplicities and strength of correlations based on the shortest distances. The blue arrows indicate the chemical shift difference between protons on the t-ring and the p-ring.

exchangeable to heavy water, proving that also in fibers surface effects may play a role. The crystallite size of Twaron1010 was not estimated, but since it is a yarn with intermediate modulus, surface effects might explain the relatively broad carbon lines despite high-power decoupling and fast spinning. The broad lines could also be due to some disorder in surface regions discussed above, or small packing variations causing varying ring current effects. The orientational distribution for fibers was estimated to approximately 10−15° by ^{2}H, ^{13}C and ^{15}N NMR.[17,19,20,61]

A detailed 2D comparison comparing the distances of the chemical shift pairs in the experimental correlation shows that the **AP** vs **P** and **L** vs **U** motifs are not clearly reflected in the 2D RMS error or the correlation pattern. Therefore, we cannot conclude on the presence of them in Twaron 1010. DFT calculations of different models, however show clear differences. The **.*.S allomorphs do not match with the chemical shift data of Twaron 1010 as evidenced in the large much larger RMS error in the 1D and 2D chemical shift comparison and therefore Twaron 1010 is mainly characterized by **.*.NS allomorphs. Since the total energies of the allomorphs are very similar, some disorder is present in PPTA fibers, as well as some orientational distribution in the packing of the crystallites, it seems likely that different allomorphs coexist in the fiber.

■ CONCLUSIONS

Systematic variation of four structural motifs encountered in literature results in a family of 16 PPTA structures with the same crystal lattice. From the energy point of view, DFT calculations show that 9 PPTA structures are energetically viable (one is similar to Liu model discussed in literature, but with $\beta \neq 90°$). All these models consists of two molecular chains in herringbone packing being either at the same height or not, having alike or unlike rings in neighboring chains next to each other and parallel or antiparallel alignment of the amide linkages in the neighboring chains. Furthermore, a slight shift along the *c*-axis of a fraction of an Å can be present. For the AP.L.NS, we find a second variant with a slightly different unit cell.

The combination of high-field solid-state NMR at fast spinning speeds (35 kHz) and DFT calculations yields the complete unambiguous assignment of ^{1}H and ^{13}C chemical shifts of an intermediate modulus PPTA fiber (Twaron 1010). The carbon assignment revises the ones in literature by English and Fukuda.[10,11] NICS calculations show that $\sigma-\pi$ bonding as well as hydrogen bonding both influence the chemical structure of the aromatic rings and account for the very similar proton chemical shifts on the p-ring.

The calculated chemical shifts for ^{1}H and ^{13}C are in best agreement with experiment for the allomorphs with the adjacent chains in the unit cell at exactly the same height: P.L.NS, P.U.NS, AP.U.NS, AP.L.NS, and AP.L.NS(II)).

Detailed 2D chemical shift comparisons confirm that for the Twaron fiber the **.*.NS allomorphs are the most likely structures. The **.*.S models yield shifts that deviate from the chemical shifts observed in experiments and also simulated correlation patterns based on the shortest distances do not agree with the correlations and the intensities observed in experiments. Comparison of the calculations show the influence of different structural motifs on the chemical shifts, however the relative large experimental line widths do not allow to conclude on the prevalence of one of them in Twaron 1010.

From the fact that no allomorph perfectly matches the experimental spectra, that the energies of the allomorphs are very

DOI: 10.1021/acs.macromol.6b01051
Macromolecules 2016, 49, 5548−5560

similar and earlier NMR studies probed some heterogeneity and orientational distribution with respect to the fiber axis, it is well possible that several (**.*.NS) allomorphs coexist in the fibers.

■ ASSOCIATED CONTENT

Supporting Information

The Supporting Information is available free of charge on the ACS Publications website at DOI: 10.1021/acs.macromol.6b01051.

Additional information on the different models including DFT of benzene (Table S1), proton and carbon chemical shift data (Tables S2−S10), fit parameters (Table S11), the lattice parameters (Tables S12 and S13), Nucleus Independent Chemical Shift (NICS) calculations (Table S14), the position of all the atoms in the unit cell (Tables S15−S23), the ^{1}H SQ-DQ correlation spectrum (Figure S1), RMS errors (Figure S2), comparison of the calculated ^{13}C and ^{1}H isotropic chemical shift with the assignment from experiments (Figures S3−S6), and constituted 2D HetCor spectra (Figures S7−S15) (PDF)

■ AUTHOR INFORMATION

Corresponding Author

*(A.P.M.K.) E-mail: a.kentgens@nmr.ru.nl Phone: +31 24 36 52078.

Author Contributions

⊥J.O.B. and P.Z. contributed equally to this study.

Notes

The authors declare no competing financial interest.

■ ACKNOWLEDGMENTS

The authors thank Teijin Aramid for the supply of the samples and René de Gelder for helpfull discussions throughout the preparation of the manuscript. This research is funded by COAST Project 053.21.101.The Netherlands Organization for Scientific Research (NWO) is acknowledged for their financial support of the solid-state NMR facility for advanced material science. The work of P.Z. and G.A.d.W. is part of the research program of the "Stichting voor Fundamenteel Onderzoek der Materie (FOM)" with financial support from the Nederlandse Organisatie voor Wetenschappelijk Onderzoek (Netherlands Organization for Scientific Research, NWO).

■ REFERENCES

(1) Northolt, M. X-ray diffraction study of poly(p-phenylene terephthalamide) fibres. *Eur. Polym. J.* **1974**, *10*, 799−804.

(2) Hasagawa, R. K.; Chatani, Y.; Tadokoro, H. *Proc. Crystallogr. Soc. Jpn.* **1973**, 21.

(3) Tashiro, K.; Kobayashi, M.; Tadokoro, H. Elastic Moduli and Molecular Structures of Several Crystalline Polymers, Including Aromatic Polyamides. *Macromolecules* **1977**, *10*, 413−420.

(4) Haraguchi, K.; Kajiyama, T.; Takayanagi, M. Uniplanar orientation of poly(p-phenylene terephthalamide) crystal in thin film and its effect on mechanical properties. *J. Appl. Polym. Sci.* **1979**, *23*, 903−914.

(5) Northolt, M. G. The structure and mechanical properties of poly(p-phenylene terephthalamide) fibre. *Br. Polym. J.* **1981**, *13*, 64−65.

(6) Liu, J.; Cheng, S.; Geil, P. Morphology and crystal structure in single crystals of poly(p-phenylene terephthalamide) prepared by melt polymerization. *Polymer* **1996**, *37*, 1413−1430.

(7) Gardner, K. H.; English, A. D.; Forsyth, V. T. New Insights into the Structure of Poly(p-phenylene terephthalamide) from Neutron Fiber Diffraction Studies. *Macromolecules* **2004**, *37*, 9654−9656.

(8) Plazanet, M.; Fontaine-Vive, F.; Gardner, K. H.; Forsyth, V. T.; Ivanov, A.; Ramirez-Cuesta, A. J.; Johnson, M. R. Neutron Vibrational Spectroscopy Gives New Insights into the Structure of Poly(p-phenylene terephthalamide). *J. Am. Chem. Soc.* **2005**, *127*, 6672−6678.

(9) Close, L. G.; Fornes, R. E.; Gilbert, R. D. A 13C NMR study of mesomorphic solutions of poly(p-phenylene terephthalamide). *J. Polym. Sci., Polym. Phys. Ed.* **1983**, *21*, 1825−1837.

(10) English, A. D. Solution and solid-state NMR characterization of poly(p-phenylene terephthalamide). *J. Polym. Sci., Part B: Polym. Phys.* **1986**, *24*, 805−815.

(11) Fukuda, M.; Kawai, H.; Horii, F.; Kitamaru, R. CP-MAS C-13 NMR-study for the characterization of water sorbed in poly(para-phenylene terephthalamide) fiber (Kevlar-49). *Polym. Commun.* **1988**, *29*, 97−99.

(12) Cain, E. J.; Gardner, K. H.; Gabara, V.; Allen, S. R.; English, A. D. Poly(p-phenyleneterephthalamide) chain dynamics. *Macromolecules* **1991**, *24*, 3721−3722.

(13) Jackson, C.; Schadt, R.; Gardner, K.; Chase, D.; Allen, S.; Gabara, V.; English, A. Dynamic structure and aqueous accessibility of poly(p-phenylene terephthalamide) crystallites. *Polymer* **1994**, *35*, 1123−1131.

(14) Schadt, R. J.; Cain, E. J.; Gardner, K. H.; Gabara, V.; Allen, S. R.; English, A. D. Terephthalamide ring dynamics of Poly(p-phenyleneterephthalamide). *Macromolecules* **1993**, *26*, 6503−6508.

(15) Schadt, R. J.; Gardner, K. H.; Gabara, V.; Allen, S. R.; English, A. D.; Chase, D. B. Dynamic structure of Poly(p-phenyleneterephthalamide). *Macromolecules* **1993**, *26*, 6509−6516.

(16) Schaefer, D. J.; English, A. D. Heterogeneous segmental dynamics of poly(p-phenyleneterephthalamide). *Polymer* **1995**, *36*, 2517−2522.

(17) Schaefer, D. J.; Schadt, R. J.; Gardner, K. H.; Gabara, V.; Allen, S. R.; English, A. D. Microscopic Dynamics and Macroscopic Mechanical Deformation of Poly(p-phenyleneterephthalamide) Fibers. *Macromolecules* **1995**, *28*, 1152−1158.

(18) McElheny, D.; Frydman, V.; Frydman, L. A solid-state 13C NMR analysis of molecular dynamics in aramide polymers. *Solid State Nucl. Magn. Reson.* **2006**, *29*, 132−141.

(19) Wilhelm, M.; de Lacroix, S. F.; Titman, J. J.; Schmidt-Rohr, K.; Spiess, H. W. The orientation distribution in an industrial sample of poly(p-phenylenetere-phthalamide) determined by two- and three-dimensional NMR techniques. *Acta Polym.* **1993**, *44*, 279−284.

(20) Sachleben, J. R.; Frydman, L. Orientational alignment in solids from bidimensional isotropic-anisotropic nuclear magnetic resonance spectroscopy: applications to the analysis of aramide fibers. *Solid State Nucl. Magn. Reson.* **1997**, *7*, 301−311.

(21) Deshmukh, Y. S.; Wilsens, C. H. R. M.; Verhoef, R.; Hansen, M. R.; Dudenko, D.; Graf, R.; Klop, E. A.; Rastogi, S. Conformational and Structural Changes with Increasing Methylene Segment Length in Aromatic-Aliphatic Polyamides. *Macromolecules* **2016**, *49*, 950−962.

(22) Northolt, M. G.; van Aartsen, J. J. Crystal and molecular-structure of Poly-(p-phenylene terephthalamide). *J. Polym. Sci., Polym. Lett. Ed.* **1973**, *11*, 333−337.

(23) Hohenberg, P.; Kohn, W. Inhomogeneous Electron Gas. *Phys. Rev.* **1964**, *136*, B864.

(24) Kohn, W.; Sham, L. J. Self-Consistent Equations Including Exchange and Correlation Effects. *Phys. Rev.* **1965**, *140*, A1133−A1138.

(25) Perdew, J. P.; Burke, K.; Ernzerhof, M. Generalized Gradient Approximation Made Simple. *Phys. Rev. Lett.* **1996**, *77*, 3865−3868.

(26) Blöchl, P. E. Projector augmented-wave method. *Phys. Rev. B: Condens. Matter Mater. Phys.* **1994**, *50*, 17953−17979.

(27) Kresse, G.; Joubert, D. From ultrasoft pseudopotentials to the projector augmented-wave method. *Phys. Rev. B: Condens. Matter Mater. Phys.* **1999**, *59*, 1758−1775.

(28) Kresse, G.; Furthmüller, J. Efficient iterative schemes for ab initio total-energy calculations using a plane-wave basis set. *Phys. Rev. B: Condens. Matter Mater. Phys.* **1996**, *54*, 11169−11186.

(29) Kresse, G.; Furthmüller, J. Efficiency of ab-initio total energy calculations for metals and semiconductors using a plane-wave basis set. *Comput. Mater. Sci.* **1996**, *6*, 15−50.

(30) Monkhorst, H. J.; Pack, J. D. Special points for Brillouin-zone integrations. *Phys. Rev. B* **1976**, *13*, 5188−5192.

DOI: 10.1021/acs.macromol.6b01051
Macromolecules 2016, 49, 5548−5560

(31) Dion, M.; Rydberg, H.; Schröder, E.; Langreth, D. C.; Lundqvist, B. I. Van der Waals Density Functional for General Geometries. *Phys. Rev. Lett.* **2004**, *92*, 246401.
(32) Thonhauser, T.; Cooper, V. R.; Li, S.; Puzder, A.; Hyldgaard, P.; Langreth, D. C. Van der Waals density functional: Self-consistent potential and the nature of the van der Waals bond. *Phys. Rev. B: Condens. Matter Mater. Phys.* **2007**, *76*, 125112.
(33) Hazrati, E.; de Wijs, G. A.; Brocks, G. Li intercalation in graphite: A van der Waals density-functional study. *Phys. Rev. B: Condens. Matter Mater. Phys.* **2014**, *90*, 155448.
(34) Klimeš, J.; Bowler, D. R.; Michaelides, A. Chemical accuracy for the van der Waals density functional. *J. Phys.: Condens. Matter* **2010**, *22*, 022201.
(35) Klimeš, J.; Bowler, D. R.; Michaelides, A. Van der Waals density functionals applied to solids. *Phys. Rev. B: Condens. Matter Mater. Phys.* **2011**, *83*, 195131. and references therein.
(36) Román-Pérez, G.; Soler, J. M. Efficient Implementation of a van der Waals Density Functional: Application to Double-Wall Carbon Nanotubes. *Phys. Rev. Lett.* **2009**, *103*, 096102.
(37) Zhang, Y.; Yang, W. Comment on "Generalized Gradient Approximation Made Simple. *Phys. Rev. Lett.* **1998**, *80*, 890−890.
(38) Lee, K.; Murray, E. D.; Kong, L.; Lundqvist, B. I.; Langreth, D. C. Higher-accuracy van der Waals density functional. *Phys. Rev. B: Condens. Matter Mater. Phys.* **2010**, *82*, 081101.
(39) Perdew, J. P.; Yue, W. Accurate and simple density functional for the electronic exchange energy: Generalized gradient approximation. *Phys. Rev. B: Condens. Matter Mater. Phys.* **1986**, *33*, 8800−8802.
(40) David, W. I. F.; Ibberson, R. M.; Jeffrey, G. A.; Ruble, J. R. The crystal structure analysis of deuterated benzene and deuterated nitromethane by pulsed-neutron powder diffraction: a comparison with single crystal neutron diffraction analysis. *Phys. B* **1992**, *180−181*, 597−600.
(41) Pickard, C. J.; Mauri, F. All-electron magnetic response with pseudopotentials: NMR chemical shifts. *Phys. Rev. B: Condens. Matter Mater. Phys.* **2001**, *63*, 245101.
(42) Yates, J. R.; Pickard, C. J.; Mauri, F. Calculation of NMR chemical shifts for extended systems using ultrasoft pseudopotentials. *Phys. Rev. B: Condens. Matter Mater. Phys.* **2007**, *76*, 024401.
(43) VASP manual, http://cms.mpi.univie.ac.at/vasp/vasp/vasp.html.
(44) Fung, B. M.; Khitrin, A. K.; Ermolaev, K. An Improved Broadband Decoupling Sequence for Liquid Crystals and Solids. *J. Magn. Reson.* **2000**, *142*, 97−101.
(45) Morcombe, C. R.; Zilm, K. W. Chemical shift referencing in MAS solid state NMR. *J. Magn. Reson.* **2003**, *162*, 479−486.
(46) Lafon, O.; Wang, Q.; Hu, B.; Trébosc, J.; Deng, F.; Amoureux, J.-P. Proton-proton homonuclear dipolar decoupling in solid-state NMR using rotor-synchronized z-rotation pulse sequences. *J. Chem. Phys.* **2009**, *130*, 014504.
(47) Rutledge, G.; Suter, U. W. Detailed atomistic simulation of oriented pseudocrystalline polymers and application to a stiff-chain aramid. *Macromolecules* **1991**, *24*, 1921−1931.
(48) Penn, L.; Larsen, F. Physicochemical properties of Kevlar 49 Fiber. *J. Appl. Polym. Sci.* **1979**, *23*, 59.
(49) Baias, M.; Widdifield, C. M.; Dumez, J.-N.; Thompson, H. P. G.; Cooper, T. G.; Salager, E.; Bassil, S.; Stein, R. S.; Lesage, A.; Day, G. M.; Emsley, L. Powder crystallography of pharmaceutical materials by combined crystal structure prediction and solid-state 1H NMR spectroscopy. *Phys. Chem. Chem. Phys.* **2013**, *15*, 8069−8080.
(50) Yates, J. R.; Pham, T. N.; Pickard, C. J.; Mauri, F.; Amado, A. M.; Gil, A. M.; Brown, S. P. An Investigation of Weak CH···O Hydrogen Bonds in Maltose Anomers by a Combination of Calculation and Experimental Solid-State NMR Spectroscopy. *J. Am. Chem. Soc.* **2005**, *127*, 10216−10220.
(51) Gowda, C. M.; Vasconcelos, F.; Schwartz, E.; van Eck, E. R. H.; Marsman, M.; Cornelissen, J. J. L. M.; Rowan, A. E.; de Wijs, G. A.; Kentgens, A. P. M. Hydrogen bonding and chemical shift assignments in carbazole functionalized isocyanides from solid-state NMR and first-principles calculations. *Phys. Chem. Chem. Phys.* **2011**, *13*, 13082−13095.
(52) Charpentier, T.; Ispas, S.; Profeta, M.; Mauri, F.; Pickard, C. J. First-Principles Calculation of 17O, 29Si, and 23Na NMR Spectra of Sodium Silicate Crystals and Glasses. *J. Phys. Chem. B* **2004**, *108*, 4147−4161.
(53) Blanc, F.; Basset, J.-M.; Copéret, C.; Sinha, A.; Tonzetich, Z. J.; Schrock, R. R.; Solans-Monfort, X.; Clot, E.; Eisenstein, O.; Lesage, A.; Emsley, L. Dynamics of Silica-Supported Catalysts Determined by Combining Solid-State NMR Spectroscopy and DFT Calculations. *J. Am. Chem. Soc.* **2008**, *130*, 5886−5900.
(54) Middlemiss, D. S.; Blanc, F.; Pickard, C. J.; Grey, C. P. Solid-state NMR calculations for metal oxides and gallates: Shielding and quadrupolar parameters for perovskites and related phases. *J. Magn. Reson.* **2010**, *204*, 1−10.
(55) Sardo, M.; Siegel, R.; Santos, S. M.; Rocha, J. a.; Gomes, J. R. B.; Mafra, L. Combining Multinuclear High-Resolution Solid-State MAS NMR and Computational Methods for Resonance Assignment of Glutathione Tripeptide. *J. Phys. Chem. A* **2012**, *116*, 6711−6719.
(56) Dervişoğlu, R.; Middlemiss, D. S.; Blanc, F.; Lee, Y.-L.; Morgan, D.; Grey, C. P. Joint Experimental and Computational 17O and 1H Solid State NMR Study of $Ba_2In_2O_4(OH)_2$ Structure and Dynamics. *Chem. Mater.* **2015**, *27*, 3861−3873.
(57) Baias, M.; Dumez, J.-N.; Svensson, P. H.; Schantz, S.; Day, G. M.; Emsley, L. De Novo Determination of the Crystal Structure of a Large Drug Molecule by Crystal Structure Prediction-Based Powder NMR Crystallography. *J. Am. Chem. Soc.* **2013**, *135*, 17501−17507.
(58) Baias, M.; Lesage, A.; Aguado, S.; Canivet, J.; Moizan-Basle, V.; Audebrand, N.; Farrusseng, D.; Emsley, L. Superstructure of a Substituted Zeolitic Imidazolate Metal-Organic Framework Determined by Combining Proton Solid-State NMR Spectroscopy and DFT Calculations. *Angew. Chem.* **2015**, *127*, 6069−6074.
(59) Charpentier, T.; Menziani, M. C.; Pedone, A. Computational simulations of solid state NMR spectra: a new era in structure determination of oxide glasses. *RSC Adv.* **2013**, *3*, 10550−10578.
(60) Harris, R. K.; Joyce, S. A.; Pickard, C. J.; Cadars, S.; Emsley, L. Assigning carbon-13 NMR spectra to crystal structures by the INADEQUATE pulse sequence and first principles computation: a case study of two forms of testosterone. *Phys. Chem. Chem. Phys.* **2006**, *8*, 137−143.
(61) Yeo, J.-H.; Demura, M.; Asakura, T.; Fujito, T.; Imanari, M.; Nicholson, L. K.; Cross, T. A. Structural analysis of highly oriented poly(p-phenylene-terephthalamide) by 15N solid-state nuclear magnetic resonance. *Solid State Nucl. Magn. Reson.* **1994**, *3*, 209−218.

DOI: 10.1021/acs.macromol.6b01051
Macromolecules 2016, 49, 5548−5560